

Feedforward Regulation Ensures Stability and Rapid Reversibility of a Cellular State

Andreas Doncic¹ and Jan M. Skotheim^{1,*}

¹Department of Biology, Stanford University, Stanford, CA 94305, USA

*Correspondence: skotheim@stanford.edu

<http://dx.doi.org/10.1016/j.molcel.2013.04.014>

SUMMARY

Cellular transitions are important for all life. Such transitions, including cell fate decisions, often employ positive feedback regulation to establish and stabilize new cellular states. However, positive feedback is unlikely to underlie stable cell-cycle arrest in yeast exposed to mating pheromone because the signaling pathway is linear, rather than bistable, over a broad range of extracellular pheromone concentration. We show that the stability of the pheromone-arrested state results from coherent feedforward regulation of the cell-cycle inhibitor Far1. This network motif is effectively isolated from the more complex regulatory network in which it is embedded. Fast regulation of Far1 by phosphorylation allows rapid cell-cycle arrest and reentry, whereas slow Far1 synthesis reinforces arrest. We expect coherent feedforward regulation to be frequently implemented at reversible cellular transitions because this network motif can achieve the ostensibly conflicting aims of arrest stability and rapid reversibility without loss of signaling information.

INTRODUCTION

A genome encodes several cellular states (or fates) distinguished by morphology or gene expression. Cells transition from one state to another in response to changing input signals that are processed by specific regulatory networks. Successful cellular transitions require that cells first commit to, and then maintain, a new cellular state. Notably, commitment has to be accurate even in the presence of environmental fluctuations and stochastic noise due to low numbers of key regulatory molecules (Balázsi et al., 2011; Di Talia et al., 2007; Johnston and Desplan, 2010). Following commitment, cells must reliably and consistently activate a state-specific gene expression program because coexpression of exclusive programs can have fatal results (Doncic et al., 2011).

Despite these shared features for all cellular transitions, we expect distinct context-dependent physiological requirements to be reflected in the associated regulatory networks. Cellular transitions may be divided into two classes: reversible and irreversible. Molecular networks regulating irreversible transitions often employ strong positive feedback loops to ensure

the stability of downstream cellular states (Jukam and Desplan, 2010). One such example of an irreversible transition is the process of *Xenopus* oocyte maturation, which can be initiated by a transient stimulus (Xiong and Ferrell, 2003). Once activated, the positive feedback loop, comprised exclusively of individually reversible chemical reactions, maintains its activity in the absence of extracellular stimulus. Increased stability of the matured state arises specifically due to irreversible positive feedback. However, this route to stability poses a problem for transitions requiring reversibility, such as cell-cycle arrest in response to DNA damage or defects in spindle assembly. Here, the twin aims of stability and reversibility appear to conflict. To determine signaling principles governing such reversible cellular states, we decided to examine pheromone arrest in budding yeast.

Upon exposure to mating pheromone (α factor), haploid yeast cells arrest the cell cycle in early G1 phase and prepare to mate (Hartwell et al., 1974). Successful mating requires a stable cell-cycle arrest to allow for altered gene expression, chemotropism, and cell fusion (Madhani, 2007). However, cells reenter the cell cycle if the extracellular pheromone is removed, as in the case when a competitor mates with the prospective partner. Thus, both stability and reversibility are required of the regulatory system governing pheromone arrest.

The conflict between cell fusion (mating) and fission (cell cycle) is reflected in mutual inhibition at the interface between the mating and the cell-cycle signaling pathways in budding yeast (Figure 1A). To select the mitotic fate, the upstream G1 cyclin Cln3 activates the cyclin-dependent kinase (CDK) to phosphorylate the transcriptional inhibitor Whi5. This initiates a positive feedback loop, centered on the downstream G1 cyclins Cln1 and Cln2, that drives entry to the cell cycle and activates the downstream B-type cyclins (Costanzo et al., 2004; de Bruin et al., 2004; Skotheim et al., 2008). Importantly, this G1 control network exhibits a hysteretic response (i.e., that outputs such as *CLN2* transcription depend on the history in the input G1 cyclin activity signal) (Charvin et al., 2010). Once activated, the positive feedback loop is irreversible and will maintain its activity despite removal of the upstream activating G1 cyclin signal. Thus, G1 control is performed by a bistable system, in which a low and a high CDK activity state are separated by a well-defined commitment point (Doncic et al., 2011). Upon commitment to cell division, the G1 cyclins target the CDK inhibitor Far1 for degradation (Gartner et al., 1998; Henchoz et al., 1997; McKinney et al., 1993) and inactivate the mating pathway scaffold protein Ste5 (Garrenton et al., 2009; Strickfaden et al., 2007). Conversely, mating arrest is effected by Far1, likely via stoichiometric inhibition of the G1 cyclin CDK complexes.

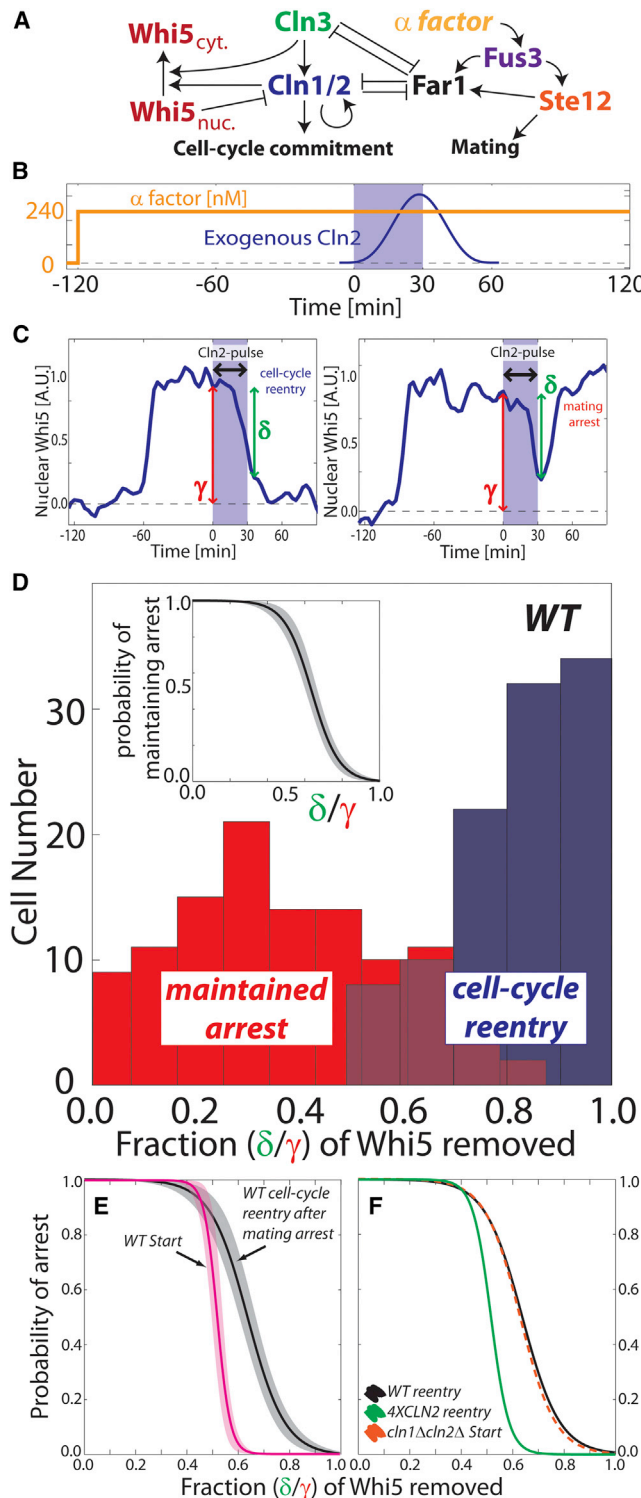


Figure 1. The CDK Threshold for Cell-Cycle Entry Is Higher for Pheromone-Arrested than Freely Cycling Cells

(A) Regulatory schematic.

(B) Experiment schematic for measuring cell-cycle reentry threshold in arrested cells expressing an exogenous Cln2 pulse from an integrated *MET3* promoter.

Upon pheromone stimulation, Far1 is feedforward-regulated by the mitogen-activated protein kinase (MAPK) Fus3 (Gartner et al., 1998; Henchoz et al., 1997; Peter et al., 1993; Tyers and Futcher, 1993). Thus, a single input activates Far1 via two distinct mechanisms: Fus3 directly phosphorylates and activates Far1 and indirectly induces Far1 expression through the transcription factor Ste12 (Oehlen et al., 1996).

The network structure that activates Far1 is called a coherent feedforward loop, and many of its theoretical properties have been elucidated (Alon, 2007; Mangan and Alon, 2003). However, network motifs always exist within the context of more complex regulatory networks (Yeager-Lotem et al., 2004), suggesting that a simplified analysis of network motifs in isolation may be of limited value. For example, as described above, the coherent feedforward regulation of Far1 by Fus3 is intertwined with the core cell-cycle pathway at multiple points, including the mutual inhibition of Far1 and the G1 cyclins as well as the inhibition of Ste5 by the G1 cyclins. In this context, the question remains as to whether the analysis of a simple network motif, such as the coherent feedforward regulation of Far1, can provide insight into the regulation of a potentially more complex cell fate decision such as the mating-mitosis switch.

While much was known about the pheromone-activated MAPK pathway, it was unclear if pheromone arrest is stabilized over time. We show here that the arrest is indeed stabilized. However, this stabilization of the pheromone-arrested state is unlikely the result of positive feedback-driven hysteresis for two reasons: first, MAPK pathway activity, as measured by Fus3 phosphorylation or Ste12-dependent transcription, is linear over a broad range of extracellular pheromone concentrations (Colman-Lerner et al., 2005; Paliwal et al., 2007; Takahashi and Pryciak, 2008; Yu et al., 2008); second, we show that pheromone pathway activity is rapidly reversible upon a sharp decrease in the extracellular pheromone concentration. Here, we show that the stability of pheromone arrest is due to the transcriptional branch of the coherent feedforward regulation of the cell-cycle inhibitor Far1. Moreover, the coherent feedforward network motif can be considered in isolation of the larger network in which it is embedded due to the stability of Far1 during pheromone arrest. The implementation of feedforward, rather than feedback, regulation allows arrest stability without affecting MAPK signaling pathway output. Maintaining a consistent and graded input-output relationship between pheromone and MAPK activity allows the cell to accurately measure the extracellular pheromone concentration while being reversibly arrested. Thus, we expect feedforward regulation

(C) For each cell, we monitor its eventual cell fate (maintain arrest or reenter cell cycle) and measure the amount of Whi5-GFP removed from the nucleus by the exogenous Cln2 pulse (δ/γ).

(D) Cell-cycle reentry probability (inset) as a function of δ/γ and the corresponding histograms for cells maintaining arrest (red) or reentering the cell cycle (blue).

(E) The amount of Whi5 export required for *Start*, the point of commitment to cell division for a freely cycling cell exposed to a step increase in pheromone (magenta; see Results for details), and the reentry threshold from (D) (black). Shaded areas denote 95% confidence intervals.

(F) The thresholds for cell-cycle reentry in WT cells (black), cells with additional *CLN2* alleles (4XCLN2; green), and *Start* in freely cycling *cln1 Δ cln2 Δ* cells (orange).

to be a key feature of regulatory networks controlling reversible cellular transitions in a wide variety of contexts.

RESULTS

Pheromone Arrest Is Reinforced

Since cell fusion requires an extended cell-cycle arrest, we hypothesized that pheromone-induced arrest is reinforced over time. In this context, reinforcement implies that it is more difficult for arrested cells to reenter the cell cycle than for cycling cells. Since cell-cycle entry is driven by CDK activity, the reinforcement model predicts that the CDK activity threshold for cell-cycle entry in pheromone-arrested cells should be higher than the corresponding threshold for cycling cells.

To determine the CDK thresholds, we required a CDK activity sensor and examined cells expressing the G1 cyclin-CDK target *WHI5* fused to green fluorescent protein (GFP) (Costanzo et al., 2004). The nuclear concentration of Whi5-GFP likely reflects G1 cyclin activity because Whi5 nuclear export is promoted by CDK phosphorylation (Kosugi et al., 2009; Taberner et al., 2009). We previously found that the dynamic range of nuclear Whi5 is ideal for the analysis of G1 cell-cycle kinetics (Doncic et al., 2011; Skotheim et al., 2008), which may be due to Whi5 phosphorylation being rate limiting for G1 progression (Costanzo et al., 2004; de Bruin et al., 2004).

We previously employed Whi5-GFP to determine the CDK threshold for entering the mitotic cell cycle for freely cycling cells (Doncic et al., 2011). Briefly, asynchronously growing cells were exposed to a step increase in pheromone (0–240 nM α factor). This allowed us to classify cells based on Hartwell's original operational definition of *Start* as the point of commitment to the cell cycle. Pre-*Start* cells at the time of pheromone addition fail to exit G1 and arrest, while post-*Start* cells complete an additional mitotic cell cycle before arresting (Hartwell et al., 1974). For yeast exposed to a step increase in pheromone concentration, *Start*, the point of commitment to division in freely cycling cells, corresponded to having exported 52% \pm 3% of the nuclear Whi5 (Doncic et al., 2011).

To determine the CDK activity threshold for cell-cycle reentry from the pheromone-arrested state, we first arrested cells using 240 nM α factor. Arrested cells are characterized by low CDK activity and a large amount of nuclear Whi5-GFP. Next, the arrested cells were forced to express a pulse of exogenous Cln2 from an integrated methionine-regulated promoter (Charvin et al., 2008), *MET3pr-CLN2*, which resulted in some of the cells reentering the cell cycle and dividing (note that we refer to these cells as wild-type [WT] in the remainder of the text even though these cells contain genomic *MET3pr-CLN2*). We measured the amount of nuclear Whi5-GFP exported in response to the pulse of exogenous Cln2 and the eventual cell fate (Figures 1B, 1C, and 1D). For cell-cycle reentry from mating arrest, 64% \pm 4% of nuclear Whi5 had to be removed compared with 52% \pm 3% for a cycling cell to progress through *Start* ($p < 10^{-4}$; Figure 1E). The increased difficulty of reentering the mitotic cell cycle after exposure to mating pheromone supports the model that pheromone arrest is reinforced.

We next focused on finding the molecular basis of arrest reinforcement. The positive feedback loop that activates transcrip-

tion of the G1 cyclins Cln1 and Cln2 is an important determinant of commitment in freely cycling cells. We thus decided to examine cell-cycle reentry from the pheromone-arrested state in cells lacking these cyclins (*cln1 Δ cln2 Δ*). The cell-cycle entry thresholds from arrest were similar in WT and *cln1 Δ cln2 Δ* cells ($p = 0.36$), suggesting complete inhibition of endogenous *CLN1* and *CLN2* during pheromone arrest. Consistent with the hypothesis that arrest reinforcement is similar to a loss of Cln1 and Cln2, the cell-cycle entry thresholds for pheromone-arrested WT cells and freely cycling *cln1 Δ cln2 Δ* cells were also indistinguishable ($p = 0.74$; Figure 1F). Next, we examined the threshold for cell-cycle reentry in cells lacking the G1 cyclin Cln3 (*cln3 Δ*), cells overexpressing *CLN2* (4XCLN2) or *FAR1* (3XFAR1), and cells containing *FAR1* and *STE5* alleles that cannot be inhibited by G1 cyclins (*FAR1-S87A* and *STE5-8A*). The results are shown in Figure S1 and Table S1. Only cells containing three additional copies of *CLN2* (4XCLN2) entered the cell cycle from pheromone arrest at a lower threshold than WT cells ($p < 10^{-4}$; Figure 1F). Taken together, these results suggest that mating arrest is reinforced primarily through increased inhibition of Cln1 and Cln2.

Cln1- and Cln2-Dependent Hysteresis in Response to Pheromone

The larger CDK threshold to reenter the cell cycle compared with freely cycling cells suggests that pheromone arrest is reinforced over time. If so, cells that have been arrested longer or previously exposed to higher pheromone concentrations should be more reluctant to enter the cell cycle. In other words, the reinforced-arrest model predicts that cells should exhibit hysteresis in response to pheromone concentration. To test if arrest duration depends on the history of exposure to mating pheromone (Moore, 1984) (i.e., exhibits hysteresis), we monitored cell-cycle reentry times after exposing cells to a brief (30 min) pulse of high-pheromone concentration (240 nM) followed by a variety of lower pheromone concentrations (Figure 2A). Cells pre-exposed to the high-concentration pulse took much longer (often more than 1 hr) to reenter the cell cycle than naive control cells exposed to the same final pheromone concentrations, but not exposed to the high-pheromone pulse. This result demonstrates hysteresis and strongly supports the reinforced-arrest model (Figures 2B, S2, and S3).

Our genetic analysis of the cell-cycle reentry threshold suggested that hysteresis results from increased inhibition of Cln1 and Cln2 in pheromone-arrested cells, which might be due to increased transcription of the CDK inhibitor *FAR1* (Chang and Herskowitz, 1990; Oehlen et al., 1996). Consistent with the hypothesis that increased Far1-dependent inhibition of CDK underlies reinforcement, *cln1 Δ cln2 Δ* and *far1 Δ cln1 Δ cln2 Δ* cells did not exhibit hysteresis (Figures 2C, S2, and S3). Moreover, these results strongly support our cell-cycle entry threshold measurements shown in Figure 1 in two ways: first, cell cycle kinetics in WT cells experiencing a high-pheromone pulse is similar to the kinetics of *cln1 Δ cln2 Δ* cells not receiving the pulse; second, cell-cycle kinetics of WT and *cln1 Δ cln2 Δ* cells receiving a high-pheromone pulse was also similar (Figures 2C, 2D, S2D, and S2G–S2J). Given an increased inhibition of Cln1 and Cln2 compared with Cln3, the latter would remain the primary activator of reentry for arrested cells. If true, we would expect cells

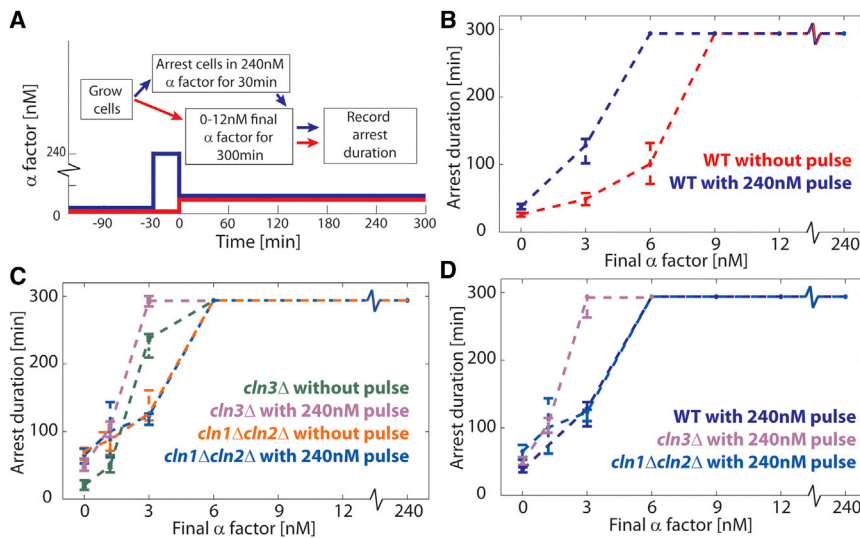


Figure 2. Hysteresis in Cell-Cycle Kinetics in Response to Changes in Pheromone Concentration

(A) Experiment schematic (see [Experimental Procedures](#)). (B) Duration of arrest in daughter cells exposed to a 30 min pulse of high-pheromone concentration or control cells. (C) Hysteresis experiment for cells lacking *Cln1*, *Cln2*, and *Cln3*. (D) Arrest duration for cells experiencing a pheromone pulse lacking either *Cln3* or *Cln1* and *Cln2*. Medians plotted with 95% confidence intervals computed using 10,000 bootstrap iterations.

lacking *CLN3* (*cln3Δ*) to reenter the cell cycle from pheromone arrest much slower than WT cells, while still being hysteretic. Indeed, this was found to be the case (Figures 2C, 2D, S2C, S2D, S3E, and S3F). Thus, the pheromone-arrested state is likely stabilized through increased Far1-dependent inhibition of *Cln1* and *Cln2* so that *Cln3* is the primary driver of cell-cycle reentry.

MAPK Pathway Activity Is Rapidly Reversible

An alternative explanation for arrest reinforcement is that MAPK activity reverses slowly upon a decrease in the extracellular pheromone concentration. To test this alternative hypothesis, we examined pathway activity in a strain expressing a *STE5-yellow fluorescent protein* (YFP) fusion protein from the endogenous locus (Yu et al., 2008). During exposure to mating pheromone, the Ste5-YFP scaffold reversibly localizes to the membrane at the shmoo tip to mediate pheromone signaling (Garrenton et al., 2009). Since membrane localization of Ste5 is required for pheromone signaling, Ste5 localization allows us to assess MAPK activity in single cells (Bush and Colman-Lerner, 2013; Strickfaden et al., 2007; Yu et al., 2008). To examine the kinetics of signaling reversibility, we grew cells in 240 nM pheromone for 2 hr and then acutely removed all pheromone. In most cells, Ste5-YFP was dissociated from the membrane within 3 min, which implies that MAPK activity is rapidly reversible (Figures 3A, 3B, and S4). To confirm this, we also examined cells expressing GFP from an integrated *FUS1* promoter (*FUS1pr-GFP*), a commonly used reporter of pheromone-induced gene expression. Consistent with rapid reversibility, we observed that the pheromone-induced transcription rate decreased in most cells within 10 min of a drop in pheromone concentration, which is on the same timescale as GFP maturation kinetics (Figures 3C and 3D). Taken together, these results imply that MAPK activity is rapidly reversible after a decrease in the extracellular pheromone concentration.

MAPK and Cell-Cycle Pathways Exhibit Noise

A hysteretic response to mating pheromone might act to buffer against fluctuations in activity in both the cell-cycle and MAPK

pathways. To estimate the potential variation in CDK activity, we measured the distribution of *CLN3* messenger RNA (mRNA) in single cells using single-molecule fluorescence in situ hybridization (FISH) (Raj et al., 2008). The number of mRNA transcripts (~5–10) is consistent with the previously observed size-independent variability in G1 duration arising due to intrinsic fluctuations associated with small numbers of molecules (Di Talia et al., 2007, 2009). Both the mean and SD of the distribution of *CLN3* mRNA molecules increased approximately 2-fold over the course of a pheromone arrest (Figures 3E and 3F), consistent with previous reports (Wittenberg et al., 1990). Since *Cln3* is a highly unstable protein with a half-life of less than 5 min (Tyers et al., 1992), we expect its concentration to track the mRNA level and exhibit significant fluctuations (Paulsson, 2004). Therefore, both the average amount of *Cln3* and the expected size of the largest *Cln3* fluctuation increase over the course of a pheromone arrest. Thus, to remain arrested, the cell is required to raise the CDK threshold for cell-cycle reentry, as we have observed.

In addition to noise in G1 cyclin levels, we suspected there might be temporal variation in the MAPK pathway activity. To test this hypothesis, we measured the amount of membrane-associated scaffold protein (Ste5-YFP) in cells arrested in 3 nM mating pheromone. We observed significant fluctuations in membrane-associated Ste5-YFP (mean coefficient of variance = 0.17, $n = 67$; Figures 3G–3I). Taken together, these results imply that significant fluctuations in both CDK and MAPK activity may also be counteracted by arrest reinforcement.

Feedforward Model for Far1 Regulation

To gain insight into how the pheromone-induced MAPK pathway can fulfill the seemingly conflicting demands of rapid reversibility and reinforced arrest, we decided to model Far1 feedforward regulation using differential equations. Our model consists of fast phosphorylation and slow transcription kinetics (see [Supplemental Experimental Procedures](#) and Figure S5 for a comprehensive analysis). The total amount of Far1 protein ($Far1^{total}$) is the sum of active ($Far1^{active}$) and inactive ($Far1^{inactive}$) fractions. Far1 is made at a rate of $f_0[\alpha(t)]$, which is a function of the extracellular pheromone concentration $\alpha(t)$. Far1 is diluted or degraded at a rate of $k_2 Far1^{total}$ (Figures 4A and 4B), so that

$$\frac{d}{dt}Far1^{total} = f_0[\alpha(t)] - k_2Far1^{total}, \quad (\text{Equation 1})$$

which after specification of the initial conditions $Far1^{total}(t=0) = F_0$ and $Far1^{active}(t=0) = 0$, can be solved to yield

$$Far1^{total} = \int_0^t f_0[\alpha(t')]e^{-k_2(t-t')}dt' + F_0e^{-k_2t}. \quad (\text{Equation 2})$$

Next, we aimed to determine the transcription rate of Far1 as a function of pheromone concentration (i.e., $f_0[\alpha(t)]$). To measure *FAR1* transcription, we constructed a strain that contains a *FAR1-Venus* fluorescent fusion protein and arrests in G1 on media containing methionine (*MET3pr-CLN2 cln1Δcln2Δcln3Δ*). Cells were arrested in G1 prior to pheromone exposure, and the concentration of Far1-Venus was tracked in individual cells through time (Figures 4C and 4D). G1-arrested cells not exposed to any pheromone expressed Far1 at a surprisingly high rate (~70% of the maximum). Additional Far1 expression was dosage-dependent with a half maximal effective concentration (EC_{50}) of ~3 nM.

To determine the stability of Far1 protein during pheromone arrest, we placed Far1-Venus expression under control of the galactose-inducible *GAL1* promoter (*GAL1pr-FAR1-Venus*). Cells were grown in media containing galactose, exposed to 240 nM mating pheromone, and then switched to media containing glucose and 3 nM pheromone. Far1-Venus concentration decreased with a half-life of ~100 min, consistent with the kinetics of dilution through cell growth, suggesting that Far1 remained completely stable during pheromone arrest (Figures 4E and 4F). Importantly, this surprising stability of Far1 during pheromone arrest validates our simplified model for the Far1 feedforward loop where complex and integrated interactions including G1 cyclin activity are absent. Thus, feedforward regulation can likely be considered insulated (Patterson et al., 2010) until cell-cycle progression leads to an increase in the activity of the downstream B-type cyclins, whose transcription is activated by Cln3 (Oehlen et al., 1998).

The stability of Far1 allows us to exploit the separate timescales of phosphorylation and growth to simplify our analysis (see Supplemental Experimental Procedures for the case with not-well-separated timescales). Far1 is activated by phosphorylation at a rate proportional to Fus3 activity, $f_1[\alpha(t)]$, and dephosphorylated by a constitutive phosphatase at a rate of k_3 , giving

$$\frac{d}{dt}Far1^{active} = f_1[\alpha(t)]Far1^{inactive} - k_3Far1^{active}. \quad (\text{Equation 3})$$

Since phosphorylation and dephosphorylation are rapid, relative to protein synthesis and dilution, Equation 2 will reach equilibrium so that

$$0 = f_1[\alpha(t)]Far1^{inactive} - k_3Far1^{active} = f_1[\alpha(t)] \times (Far1^{total} - Far1^{active}) - k_3Far1^{active}, \quad (\text{Equation 4})$$

which can be rearranged and combined with Equation 2 to yield

$$Far1^{active}(t) = \frac{f_1[\alpha(t)]}{f_1[\alpha(t)] + k_3}Far1^{total} = \frac{f_1[\alpha(t)]}{f_1[\alpha(t)] + k_3} \times \left(\int_0^t f_0[\alpha(t')]e^{-k_2(t-t')}dt' + F_0e^{-k_2t} \right). \quad (\text{Equation 5})$$

To gain insight into how the active fraction of the total Far1 changes with pheromone concentration, we decided to examine cell-cycle reentry kinetics in a variety of pheromone concentrations for cells with the same amount of Far1 protein. To do this, we exposed cells containing Far1 under exclusive control by the *GAL1* promoter to 240 nM mating pheromone while growing in galactose and then switched to glucose media containing a variable amount of pheromone (Figures 4G and 4H). Next, we measured the duration of pheromone arrest as a function of the final pheromone concentration. Arrest duration increased steadily until saturation at ~6–9 nM pheromone, again suggesting an EC_{50} of ~3 nM, similar to that for *FAR1* transcription. Taken together, our results support the alignment of MAPK activity and pheromone-induced transcription dose-response curves, which has been suggested to improve the transmission of information through the MAPK pathway (Yu et al., 2008).

The solution of our model for a step increase followed by a step decrease in pheromone is informative (Figures 4B and S5G). Upon the step increase, the initial amount of Far1 (F_0) is phosphorylated rapidly at a rate of $\sim f_1[\alpha(t)]$. Thus, the nonzero initial condition for total Far1 identified by McKinney et al. (1993) is crucial for a rapid arrest in response to mating pheromone. Next, during the period of high pheromone activity, both total and active Far1 accumulate at the slower synthesis rate of $f_0[\alpha(t)]$ to reinforce the arrested state. Finally, upon decreasing the pheromone concentration, Far1 is rapidly dephosphorylated at a rate of k_3 , leading to a sharp drop in the active fraction that can result in rapid cell-cycle reentry. Notably, Far1 is diluted at a rate of k_2 associated with cell growth. In conclusion, fast phosphorylation kinetics determines the proportion of active Far1 to allow rapid cell-cycle arrest and reentry in response to pheromone removal, whereas slower, history-dependent synthesis underlies arrest reinforcement. Specifically, our model predicts that (1) Far1 accumulates over the course of a pheromone arrest, (2) the total amount of Far1 correlates with arrest stability, and (3) removing pheromone-dependent *FAR1* transcription removes hysteresis.

Far1 Accumulation Underlies Arrest Stability

To test if Far1 accumulation might cause arrest reinforcement, we measured the amount of Far1 in live cells expressing *FAR1* fused with the Venus yellow fluorescent protein from the endogenous locus. This Venus fusion protein did not affect arrest kinetics (Figures S6A and S6B). Upon addition of pheromone, Far1-Venus initially accumulated at a constant rate for over 1 hr before asymptotically approaching its final level (Figures 5A and 5B). This matched the result from solving Equation (2) for a step increase in mating pheromone and assuming that the initial amount of Far1 is significantly less than the final concentration. Thus, a model of constant synthesis rate balanced by a dilution rate due to cell growth fits the observed Far1-Venus

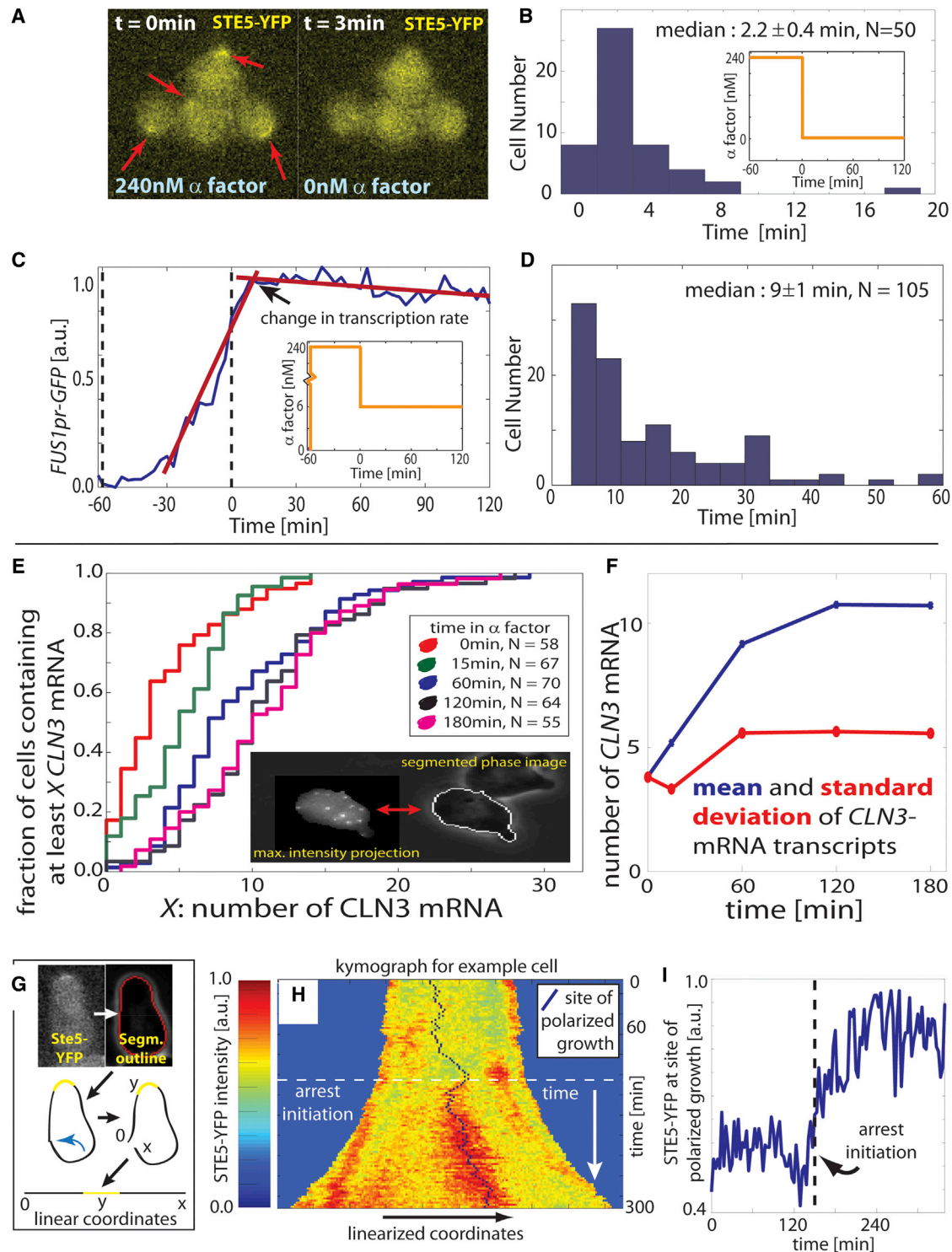


Figure 3. Mating Pathway Activity Is Rapidly Reversible, and the Cell-Cycle and MAPK Pathways Exhibit Noise

(A) Micrographs of STE5-YFP cells before and after pheromone removal (red arrows indicate shmoo tips).

(B) Histogram of the time of Ste5 membrane dissociation marking MAPK pathway inactivation. x axis denotes time between pheromone removal and the disappearance of half of the shmoo-tip-associated Ste5-YFP.

(C and D) We used the pheromone-induced *FUS1* promoter to drive expression of green fluorescent protein to measure the kinetics of mating-pathway-dependent transcription when cells arrested in 240 nM α factor were exposed to a step decrease to 6 nM α factor (inset). Time of transcription-rate change was measured (C) and displayed in a histogram (D) indicating rapid downregulation of mating-pathway-dependent transcription.

(legend continued on next page)

accumulation curves (equation and fit shown in Figure 5B). This suggests that the Far1 synthesis rate, and therefore the pathway activity, is relatively constant over the course of a pheromone arrest and unaffected by transcriptional or posttranscriptional feedback on signaling components or changes in cell morphology.

Far1 amounts at the end of a high-pheromone pulse show significant cell-to-cell variation due to differences in transcription rate and arrest duration (Colman-Lerner et al., 2005). Our model predicts that Far1-Venus levels will correlate with arrest stability. To test this, we examined arrest duration in cells experiencing a high-pheromone pulse followed by a lower, 3 nM pheromone concentration. We estimated the amount of Far1-Venus at the time of the step decrease in pheromone as the amount at the time when we detected a drop in the Far1-Venus accumulation rate approximately 50 min later (Figures 5C and S6C). In agreement with our model, cells containing more Far1-Venus arrested longer (Figures 5D and 5E and Table S2). A substantial amount of the residual variability in this relationship is due to cell size variation (Figure S6D). However, cell type (mother or daughter) does not have a size-independent effect on reentry kinetics, implying that differential expression of *CLN3* due to the daughter-specific transcription factors Ace2 and Ash1 (Di Talia et al., 2009) is not maintained through a pheromone arrest.

In addition, the correlation between arrest duration and Far1 amount remained unchanged in *cln1Δcln2Δ* and WT cells, again implying that cell-cycle reentry is primarily driven by Cln3 in competition with Far1 (Figure 5F). Consistent with Cln3 as the main driver of cell-cycle reentry, arrest of *cln3Δ* cells was approximately 2 hr longer than that of WT cells for the equivalent amount of Far1 (Figures 5G, 5I, and S6E). To test whether the observed insulation of Far1 in arrested cells (Figures 4E and 4F) is related to the activation of the B-type cyclins, we also compared Far1 abundance and arrest duration in a strain lacking the S phase cyclins *CLB5* and *CLB6* (Epstein and Cross, 1992; Schwob and Nasmyth, 1993). In agreement with this hypothesis, we see that given the same amount of Far1, *clb5Δclb6Δ* cells arrest significantly longer than WT cells (Figures 5H and 5I), demonstrating an important role for Clb5 and Clb6 at cell-cycle reentry.

Our results so far suggest that MAPK-induced *FAR1* transcription is the molecular basis of history-dependent arrest reinforcement. Indeed, the relationship between Far1 abundance and arrest duration was unchanged by doubling the duration of the pheromone pulse from 30 to 60 min, despite a significant increase in the mean arrest times (Figure 5E). The finding that cells with an equivalent amount of Far1-Venus, but different pheromone histories, arrest for similar durations implies that history dependence arises primarily from Far1 accumulation.

Decoupling *FAR1* Transcription from Pheromone Signaling Removes History Dependence

To determine if Far1 transcription is the underlying mechanism for hysteresis, we decoupled *FAR1* transcription from pathway activity by placing *FAR1* under control of a galactose-inducible promoter (*GAL1pr-FAR1*; Figure 6A). Importantly, this is the only *FAR1* allele in this strain. Next, we repeated the hysteresis experiment (Figure 2A) for cells that have equivalent amounts of Far1 but are exposed to different pheromone histories (Figure 6B). Consistent with Far1 transcription underlying history-dependent cell-cycle reentry, *GAL1pr-FAR1* cells did not exhibit hysteresis (Figures 6C and S7A–S7C). To control for the potential effect of the *FAR1* turnoff, we performed the same experiment with galactose as the sole carbon source, using a lower final pheromone concentration (1 nM) as the *GAL1* promoter overexpressed *FAR1* (Figure 6D). Again, all history dependence vanished (Figures 6E, S7D, and S7E). When *FAR1* transcription is independent of pheromone concentration, cell-cycle reentry kinetics are likely determined by current, not past, MAPK activity. Thus, we conclude that most, if not all, history dependence in this cellular decision arises due to Far1 accumulation rather than the accumulation of any other Ste12 targets (Roberts et al., 2000).

DISCUSSION

Isolation and Interrogation of an Embedded Network Motif

Understanding the potentially dynamic mechanisms underlying cellular decisions requires accurate measurement and control of input signals. Microfluidic devices coupled with fluorescence imaging allows such temporal control and quantification of signaling inputs (Berg and Block, 1984; Charvin et al., 2008; Gómez-Sjöberg et al., 2007; Hersen et al., 2008; Lee et al., 2008; Mettetal et al., 2008; Taylor et al., 2009). Here, we temporally control the pheromone input signal to show that the decision to reenter the cell cycle is based not solely on MAPK pathway activity, but also on its integrated history.

Our empirical finding that a specific network motif embedded in a larger regulatory network can be independently analyzed and is responsible for cell-cycle reentry control was not a priori obvious. Rather, one might expect that the multiple inhibitory interactions between Far1 and the G1 cyclins would necessitate a more complex model to analyze mating arrest. However, we found that negative regulation of Far1 by G1 cyclins was negligible during pheromone arrest and that Far1 inhibition is most likely executed by B-type cyclins, implying that a modular analysis focusing exclusively on the feedforward regulation of Far1 is valid all the way up to the point of B-type cyclin activity. This hopeful result suggests that signal processing properties of

(E) Single-molecule FISH was used to count the number of *CLN3* mRNA in individual cells through a 3 hr pheromone arrest using maximum intensity projections of a z stack (inset).

(F) Both the mean and standard distribution of *CLN3* mRNA increases during arrest.

(G) *STE5-YFP* cells containing an integrated scaffold fusion protein were segmented, and the boundary coordinates were linearized.

(H) Upon exposure to 3 nM pheromone, Ste5-YFP is recruited to the membrane. Each horizontal line of the kymograph shows the YFP fluorescence at the membrane in the linearized coordinate system at a specific time. The length of the cell boundary increases with time; blue color denotes non-cell.

(I) Example cell for which the level of Ste5 recruited to the shmoo tip fluctuates over the course of the pheromone arrest, implying fluctuations in MAPK activity.

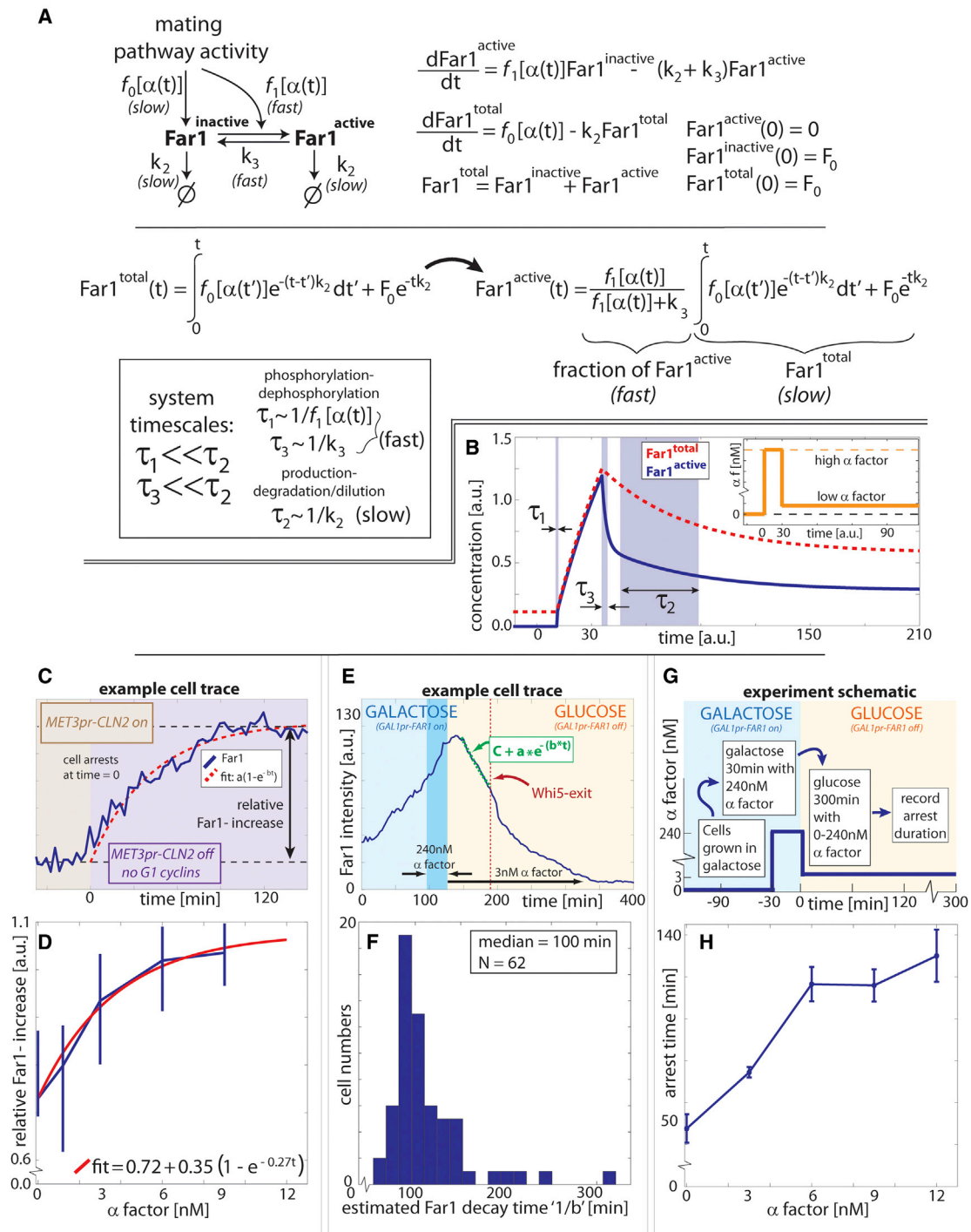


Figure 4. Feedforward Model for Far1 Synthesis and Activation

(A) A mathematical model and analytical solution for feedforward regulation of Far1 (see Results). A separation of fast phosphorylation (τ_1) and dephosphorylation (τ_3) timescales relative to a slow synthesis (τ_2) timescale allows a simplification of the expression for $\text{Far1}^{\text{active}}$.

(B) Solution for total and active Far1 illustrating the response to two step changes in pheromone concentration (inset).

(C) Far1-Venus expression was measured in G1-arrested *cln1 Δ cln2 Δ cln3 Δ MET3pr-CLN2* cells exposed to a range of pheromone concentration.

(D) Median increase in Far1-Venus \pm 95% bootstrap confidence intervals as a function of pheromone concentration. $N_{0\text{nM}} = 20$, $N_{1.2\text{nM}} = 21$, $N_{3\text{nM}} = 26$, $N_{6\text{nM}} = 26$, and $N_{9\text{nM}} = 15$.

(E) Cells with their endogenous Far1 promoter replaced by a *GAL1* promoter (cf. Figure 6A) were grown in galactose and exposed to a brief (30 min) pulse of 240 nM α factor, after which the carbon source was shifted to glucose media containing 3 nM mating pheromone (*GAL1pr-FAR1-Venus* off).

(legend continued on next page)

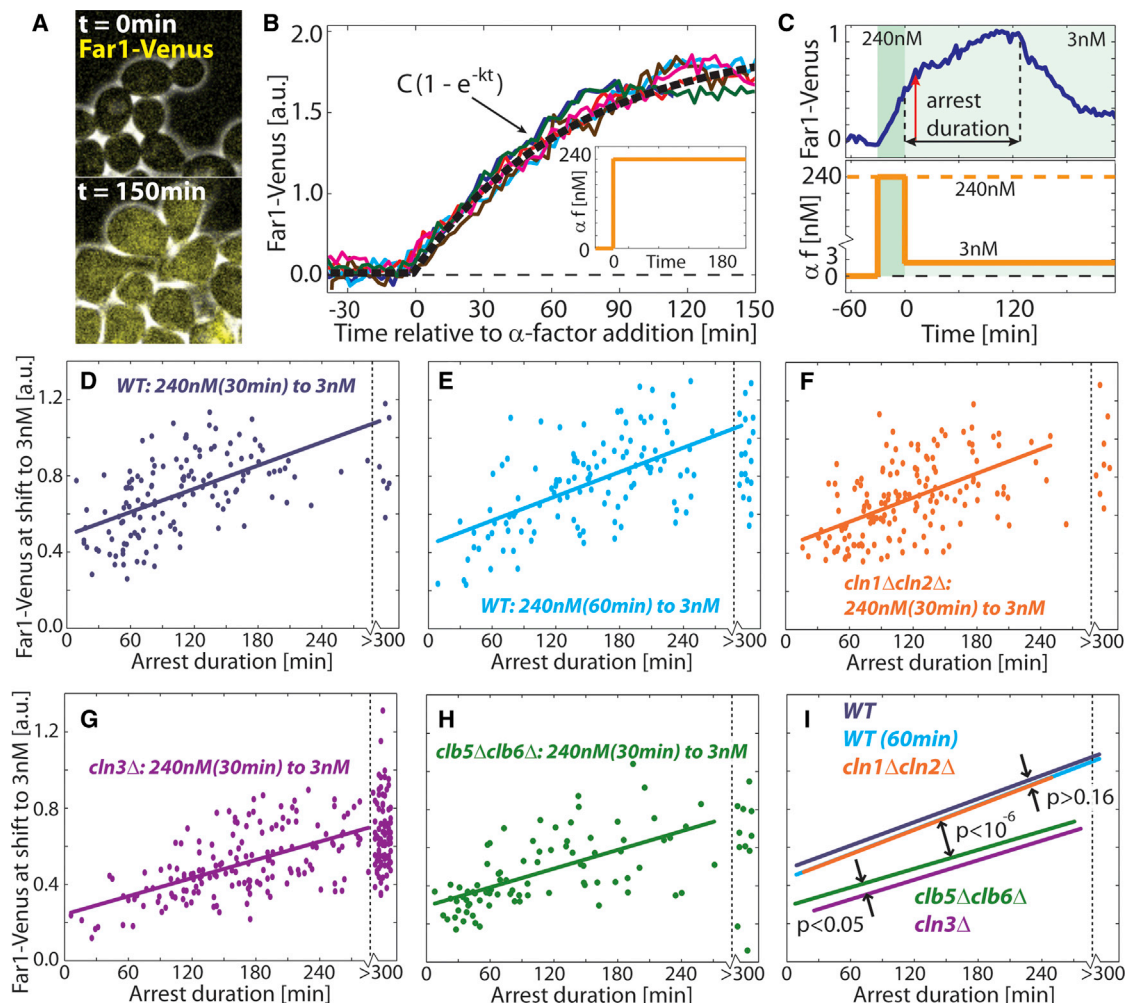


Figure 5. Far1-Venus Abundance Correlates with Arrest Duration

(A) Composite phase and fluorescence images of Far1-Venus in cells exposed to a step increase in pheromone.

(B) Single-cell measurements of Far1-Venus in cells exposed to a step increase in pheromone (inset).

(C) Arrest duration (dashed lines determined by Whi5-mCherry nuclear residence) and Far1 abundance after the high-pheromone pulse (red arrow) were measured.

(D–I) Arrest duration correlated with Far1 abundance for WT cells experiencing 30 min (D) or 60 min (E) pulses of high pheromone, *cln1Δcln2Δ* (30 min) (F), *cln3Δ* (30 min) (G), and *clb5Δclb6Δ* cells (30 min) (H). Comparison shown in (I). The R^2 values for these correlations are as follows: WT (30 min) = 0.32, WT (60 min) = 0.37, *cln1Δcln2Δ* = 0.29, *cln3Δ* = 0.35, and *clb5Δclb6Δ* = 0.37.

specific network motifs may be usefully applied even within the context of much more complex regulatory networks.

Initial Condition of Nonzero Far1 Allows Fast Activation

We find that coherent feedforward regulation of Far1 ensures a robust, yet rapidly reversible, cellular state. Far1 accumulates slowly to ensure stability against fluctuations and size-dependent increases in Cln3 activity (Turner et al., 2012), whereas fast phosphorylation cycles allow rapid responses. Regulation

of mating arrest is most similar to coherent feedforward regulation with a logical AND gate previously analyzed theoretically by Mangan and Alon (2003). In that analysis, an initial condition of no output protein yields a solution in which both fast and slow positively regulating branches combine for slow activation and fast inactivation. In sharp contrast, the initial condition of nonzero Far1 in early G1 prior to pheromone exposure (McKinney et al., 1993) allows rapid activation above the threshold required for cell-cycle arrest.

(F) Histogram of Far1-Venus concentration half-life estimates suggests Far1 is stable and diluted by cell growth. An exponential function was fit to the Far1 decay curve between the time of initial Far1 decrease and Whi5-nuclear exit (red dashed line).

(G) Schematic of experiment to measure arrest duration in cells containing equivalent amounts of Far1 protein exposed to different pheromone concentrations.

(H) Arrest duration (mean \pm SEM) for cells treated as shown in (G). $N_{0nM} = 28$, $N_{3nM} = 96$, $N_{6nM} = 43$, $N_{9nM} = 40$, and $N_{12nM} = 28$.

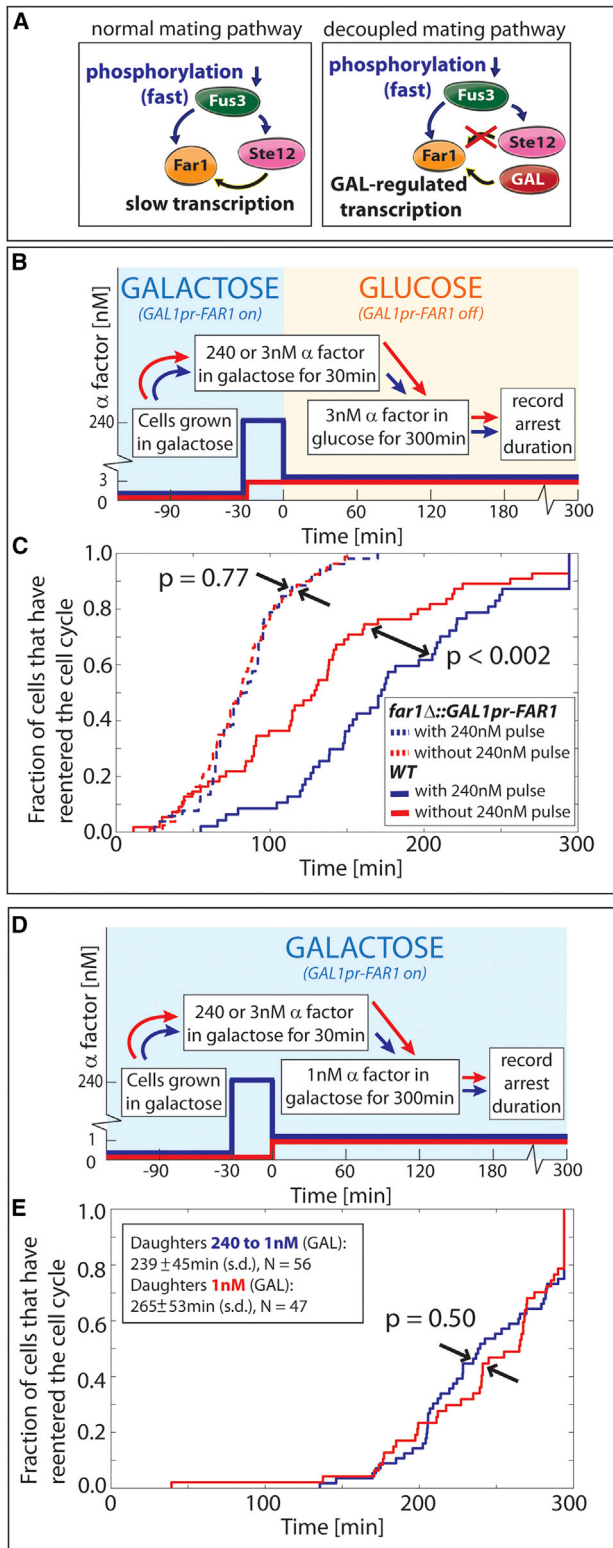


Figure 6. Exogenous Phormone-Independent Control of FAR1 Transcription Eliminates Hysteresis

(A–C) Motif (A) and experiment (B) schematic for the distributions of arrest duration shown in (C) for cells expressing FAR1 from the galactose-inducible

Feedforward Regulation Balances Tradeoffs

Feedforward regulation may produce sign-sensitive delays, non-monotone responses, pulse generation, and fold-change detection (Yosef and Regev, 2011). Moreover, a recent study suggests the presence of widespread feedforward regulation in yeast cell-cycle control (Csikász-Nagy et al., 2009). However, the physiological function of these proposed feedforward networks remains to be tested experimentally, and transitions to reinforced cellular states have mostly been attributed to positive feedback mechanisms, especially if the transition is irreversible (Charvin et al., 2010; Xiong and Ferrell, 2003).

In reversible cellular transitions, feedforward regulation may provide a superior architecture to balance response kinetics and stability compared to positive feedback loops, which can be difficult to reverse. Moreover, even when positive feedback loops are reversible, as in the case of mitosis, stable cellular states are generated through bistability (Pomerening et al., 2003; Sha et al., 2003). Bistability implies a multivalued input-output relationship that, in turn, necessarily implies a loss of information about the input signal. In sharp contrast, feedforward regulation does not compromise the linear input-output relationship measuring the extracellular environment through the entire duration of a pheromone arrest (Bush and Colman-Lerner, 2013; Paliwal et al., 2007; Takahashi and Pryciak, 2008; Yu et al., 2008). Thus, feedforward regulation is the only network structure that achieves the twin aims of stability and reversibility with minimal tradeoffs (Figures 7A, S4, and S8, Tables S3 and S4, and Supplemental Experimental Procedures).

Separation of Timescales and Modularity

The era of genomics has produced an explosion of data on inter- and intrasignaling pathway protein interactions. Cellular networks appear highly interconnected, complex, and unlikely to be amenable to standard techniques. Yet, classical genetics and biochemistry have been successfully applied to individual, isolated signaling pathways. This is likely due to two (often neglected) simplifying facts about biological regulatory networks. First, real chemical interactions have varying strengths, in contrast to the common tendency to depict them as binary (either an interaction exists or not). If the activity of a signaling molecule with many upstream interactions could be determined by just one or two key regulators, the network can be effectively simplified by neglecting the weaker interactions. Second, networks often contain signaling events, such as phosphorylation (fast) and transcription (slow), which occur on separate timescales. From the point of view of fast events, slower events are essentially static and can be treated as such during mathematical analysis, as shown in our analysis of Far1 regulation. The separation of timescales, a standard technique of applied

GAL1 promoter (GAL1pr-FAR1) and WT control cells. Upon the carbon source switch at $t = 0$, Far1 synthesis is turned off.

(D and E) Experiment schematic (D) for the distributions of arrest duration shown in (E) for GAL1pr-FAR1 cells. In contrast to the results shown in (C), Far1 synthesis is constitutive throughout the experiment shown in (D) and (E). Results are shown for daughter cells only; similar results for mother cells are shown in Figure S7. p values were calculated using a Kolmogorov-Smirnov test.

Molecular Cell

Feedforward-Regulated Reversible Cellular State

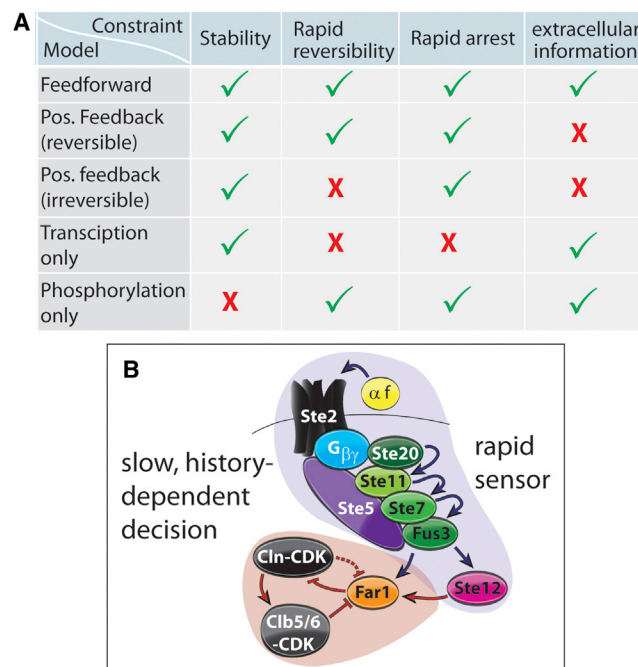


Figure 7. Coherent Feedforward Regulation Achieves All Physiological Objectives without Tradeoffs

(A) Alternative models for Far1 control are unable to achieve all the physiological objectives associated with pheromone arrest. (B) Modular architecture of a cellular decision: a rapid sensing module measures extracellular pheromone while a slow, history-dependent decision module determines cell fate.

mathematics, greatly simplifies differential equation analysis and clarifies the function of specific network interactions (Alexander et al., 2009; Bender and Orszag, 1999; Rust et al., 2007).

Here, the separation of timescales yields a modular network structure where the sensor module is independent from the decision-making module (Figure 7B). The shortest time for a cell to arrest the cell cycle is determined by the fast phosphorylation rate of the initial Far1 by the MAPK Fus3. Similarly, the fastest time to reenter the cell cycle after pheromone arrest is determined by the fast dephosphorylation and inactivation of Far1. Arrest reinforcement is determined by the slower transcription and dilution rates. Had the kinetics of all these interactions been similar, the determination of arrest, reentry, and reinforcement kinetics would be much less modular. Intriguingly, since transcription is likely to be slower than phosphorylation for fundamental biochemical reasons within most signaling pathways, we expect to see much more timescale-dependent modularity.

In engineered systems, modularity is commonly used so that individual components perform a set of limited functions, whose few parameters can be independently and easily tuned. Within the context of cell signaling, a separation of timescales results in functional modularity of specific biochemical interactions and network motifs. That specific interactions can be associated with specific functions may allow evolution to

quickly and independently select on multiple aspects of cell physiology.

EXPERIMENTAL PROCEDURES

Microscopy, Microfluidics, and Image Analysis

We used a CellASIC flow cell with Y4C plates as described in Doncic et al. (2011) unless denoted otherwise. *WHI5-mCherry* strains were exposed for 750 ms using the Colibri 540-80 LED module at 25% power. *FAR1-Venus* was exposed for 300 ms using the Colibri 505 LED module at 25% power. Image analysis was performed as described in Doncic et al. (2013). Far1-Venus at the pheromone shift (Figures 5C–5I) was taken as the point where the rate of accumulation changed (red arrow; Figures 5C and 5G), rather than the time of pheromone reduction, due to Venus maturation kinetics (Charvin et al., 2008). Single-molecule FISH was performed as in Raj et al. (2008), and mRNA numbers were determined from maximum intensity projections of z stacks containing nine slices. All strains used are congenic with W303 (see Table S4). Arrest probabilities in Figures 1D–1F and S1 were calculated using logistic regression. Confidence intervals were calculated using 10,000 bootstrap iterations.

Measurement of Cell-Cycle Reentry

Cells were grown in the flow cell in synthetic complete yeast media with 2% glucose (SCD) for at least 90 min and then arrested in SCD + 240 nM α factor. After a 2 hr arrest, we switched the medium to SCD – met + 240 nM α factor to induce expression of exogenous Cln2 from an integrated *MET3pr-CLN2* construct. Next, we switched the media back to SCD + 240 nM α factor, which ended the exogenous Cln2 pulse. We monitored the cells for an additional 2 hr to determine cell fate. Pulse durations varied between 9 and 45 min to express variable amounts of exogenous Cln2. For cells remaining arrested, the *Whi5*-GFP signal reverts to the pre-pulse level, and we define δ using the minimum amount of nuclear *Whi5*-GFP. For cells that commit, we define δ using the minimum *Whi5*-GFP value between 3 and 9 min after the end of the pulse, which corresponds approximately to the time (~5 min) it takes to inactivate the *MET3* promoter (Charvin et al., 2008). γ is defined as the nuclear *Whi5*-GFP amount at the time of methionine removal.

Hysteresis Measurement

Pre-Start G1 durations for cells experiencing a pulse of high α factor were measured from the time of the switch to the final α factor concentration to the time (half-max) when *Whi5* leaves the nucleus. For cells not experiencing the high-pheromone pulse, we score the first pre-Start G1 duration after pheromone addition as the amount of time *Whi5* spends in the nucleus. *Whi5* nuclear entry is defined as the time point at which the nuclear *Whi5* reaches half the eventual maximum, which precedes division by 6–9 min. Nuclear exit is defined as the point at which half the maximum amount of nuclear *Whi5* has been excluded from the nucleus. Cells arrested at the movie limit were scored as being arrested for the full 294 min (max arrest).

SUPPLEMENTAL INFORMATION

Supplemental Information includes eight figures, five tables, and Supplemental Experimental Procedures and can be found with this article online at <http://dx.doi.org/10.1016/j.molcel.2013.04.014>.

ACKNOWLEDGMENTS

We thank A. Amodeo, A. Colman-Lerner, F. Cross, R. Lee, M. Loog, P. Pryciak, E. Siggia, and C. Gomez for insightful comments; E. Lui and R. Yu for reagents; and J. Turner for assistance with the FISH assay. Research was funded by the Burroughs Wellcome Fund and the NIH (GM092925).

Received: October 18, 2012
Revised: January 28, 2013
Accepted: April 9, 2013
Published: May 16, 2013

REFERENCES

- Alexander, R.P., Kim, P.M., Emonet, T., and Gerstein, M.B. (2009). Understanding modularity in molecular networks requires dynamics. *Sci. Signal.* 2, pe44.
- Alon, U. (2007). Network motifs: theory and experimental approaches. *Nat. Rev. Genet.* 8, 450–461.
- Balázsi, G., van Oudenaarden, A., and Collins, J.J. (2011). Cellular decision making and biological noise: from microbes to mammals. *Cell* 144, 910–925.
- Bender, C.M., and Orszag, S.A. (1999). *Advanced mathematical methods for scientists and engineers* (New York: Springer).
- Berg, H.C., and Block, S.M. (1984). A miniature flow cell designed for rapid exchange of media under high-power microscope objectives. *J. Gen. Microbiol.* 130, 2915–2920.
- Bush, A., and Colman-Lerner, A. (2013). Quantitative measurement of protein relocalization in live cells. *Biophys. J.* 104, 727–736.
- Chang, F., and Herskowitz, I. (1990). Identification of a gene necessary for cell cycle arrest by a negative growth factor of yeast: FAR1 is an inhibitor of a G1 cyclin, CLN2. *Cell* 63, 999–1011.
- Charvin, G., Cross, F.R., and Siggia, E.D. (2008). A microfluidic device for temporally controlled gene expression and long-term fluorescent imaging in unperturbed dividing yeast cells. *PLoS ONE* 3, e1468.
- Charvin, G., Oikonomou, C., Siggia, E.D., and Cross, F.R. (2010). Origin of irreversibility of cell cycle start in budding yeast. *PLoS Biol.* 8, e1000284.
- Colman-Lerner, A., Gordon, A., Serra, E., Chin, T., Resnekov, O., Endy, D., Pesce, C.G., and Brent, R. (2005). Regulated cell-to-cell variation in a cell-fate decision system. *Nature* 437, 699–706.
- Costanzo, M., Nishikawa, J.L., Tang, X., Millman, J.S., Schub, O., Breitkreuz, K., Dewar, D., Rupes, I., Andrews, B., and Tyers, M. (2004). CDK activity antagonizes Whi5, an inhibitor of G1/S transcription in yeast. *Cell* 117, 899–913.
- Csikász-Nagy, A., Kapuy, O., Tóth, A., Pál, C., Jensen, L.J., Uhlmann, F., Tyson, J.J., and Novák, B. (2009). Cell cycle regulation by feed-forward loops coupling transcription and phosphorylation. *Mol. Syst. Biol.* 5, 236.
- de Bruin, R.A., McDonald, W.H., Kalashnikova, T.I., Yates, J., 3rd, and Wittenberg, C. (2004). Cln3 activates G1-specific transcription via phosphorylation of the SBF bound repressor Whi5. *Cell* 117, 887–898.
- Di Talia, S., Skotheim, J.M., Bean, J.M., Siggia, E.D., and Cross, F.R. (2007). The effects of molecular noise and size control on variability in the budding yeast cell cycle. *Nature* 448, 947–951.
- Di Talia, S., Wang, H., Skotheim, J.M., Rosebrock, A.P., Fitcher, B., and Cross, F.R. (2009). Daughter-specific transcription factors regulate cell size control in budding yeast. *PLoS Biol.* 7, e1000221.
- Doncic, A., Falleur-Fettig, M., and Skotheim, J.M. (2011). Distinct interactions select and maintain a specific cell fate. *Mol. Cell* 43, 528–539.
- Doncic, A., Eser, U., Atay, O., and Skotheim, J.M. (2013). An algorithm to automate yeast segmentation and tracking. *PLoS ONE* 8, e57970.
- Epstein, C.B., and Cross, F.R. (1992). CLB5: a novel B cyclin from budding yeast with a role in S phase. *Genes Dev.* 6, 1695–1706.
- Garrenton, L.S., Braunwarth, A., Irniger, S., Hurt, E., Künzler, M., and Thorner, J. (2009). Nucleus-specific and cell cycle-regulated degradation of mitogen-activated protein kinase scaffold protein Ste5 contributes to the control of signaling competence. *Mol. Cell. Biol.* 29, 582–601.
- Gartner, A., Jovanović, A., Jeoung, D.I., Bourlat, S., Cross, F.R., and Ammerer, G. (1998). Pheromone-dependent G1 cell cycle arrest requires Far1 phosphorylation, but may not involve inhibition of Cdc28-Cln2 kinase, in vivo. *Mol. Cell. Biol.* 18, 3681–3691.
- Gómez-Sjöberg, R., Leyrat, A.A., Pirone, D.M., Chen, C.S., and Quake, S.R. (2007). Versatile, fully automated, microfluidic cell culture system. *Anal. Chem.* 79, 8557–8563.
- Hartwell, L.H., Culotti, J., Pringle, J.R., and Reid, B.J. (1974). Genetic control of the cell division cycle in yeast. *Science* 183, 46–51.
- Henchoz, S., Chi, Y., Catarin, B., Herskowitz, I., Deshaies, R.J., and Peter, M. (1997). Phosphorylation- and ubiquitin-dependent degradation of the cyclin-dependent kinase inhibitor Far1p in budding yeast. *Genes Dev.* 11, 3046–3060.
- Hersen, P., McClean, M.N., Mahadevan, L., and Ramanathan, S. (2008). Signal processing by the HOG MAP kinase pathway. *Proc. Natl. Acad. Sci. USA* 105, 7165–7170.
- Johnston, R.J., Jr., and Desplan, C. (2010). Stochastic mechanisms of cell fate specification that yield random or robust outcomes. *Annu. Rev. Cell Dev. Biol.* 26, 689–719.
- Jukam, D., and Desplan, C. (2010). Binary fate decisions in differentiating neurons. *Curr. Opin. Neurobiol.* 20, 6–13.
- Kosugi, S., Hasebe, M., Tomita, M., and Yanagawa, H. (2009). Systematic identification of cell cycle-dependent yeast nucleocytoplasmic shuttling proteins by prediction of composite motifs. *Proc. Natl. Acad. Sci. USA* 106, 10171–10176.
- Lee, P.J., Helman, N.C., Lim, W.A., and Hung, P.J. (2008). A microfluidic system for dynamic yeast cell imaging. *Biotechniques* 44, 91–95.
- Madhani, H.D. (2007). From a to [alpha]: yeast as a model for cellular differentiation (Cold Spring Harbor, NY: Cold Spring Harbor Laboratory Press).
- Mangan, S., and Alon, U. (2003). Structure and function of the feed-forward loop network motif. *Proc. Natl. Acad. Sci. USA* 100, 11980–11985.
- McKinney, J.D., Chang, F., Heintz, N., and Cross, F.R. (1993). Negative regulation of FAR1 at the start of the yeast cell cycle. *Genes Dev.* 7, 833–843.
- Mettetal, J.T., Muzzey, D., Gómez-Urbe, C., and van Oudenaarden, A. (2008). The frequency dependence of osmo-adaptation in *Saccharomyces cerevisiae*. *Science* 319, 482–484.
- Moore, S.A. (1984). Yeast cells recover from mating pheromone alpha factor-induced division arrest by desensitization in the absence of alpha factor destruction. *J. Biol. Chem.* 259, 1004–1010.
- Oehlen, L.J., McKinney, J.D., and Cross, F.R. (1996). Ste12 and Mcm1 regulate cell cycle-dependent transcription of FAR1. *Mol. Cell. Biol.* 16, 2830–2837.
- Oehlen, L.J., Jeoung, D.I., and Cross, F.R. (1998). Cyclin-specific START events and the G1-phase specificity of arrest by mating factor in budding yeast. *Mol. Gen. Genet.* 258, 183–198.
- Paliwal, S., Iglesias, P.A., Campbell, K., Hilioti, Z., Groisman, A., and Levchenko, A. (2007). MAPK-mediated bimodal gene expression and adaptive gradient sensing in yeast. *Nature* 446, 46–51.
- Patterson, J.C., Klimentko, E.S., and Thorner, J. (2010). Single-cell analysis reveals that insulation maintains signaling specificity between two yeast MAPK pathways with common components. *Sci. Signal.* 3, ra75.
- Paulsson, J. (2004). Summing up the noise in gene networks. *Nature* 427, 415–418.
- Peter, M., Gartner, A., Horecka, J., Ammerer, G., and Herskowitz, I. (1993). FAR1 links the signal transduction pathway to the cell cycle machinery in yeast. *Cell* 73, 747–760.
- Pomerening, J.R., Sontag, E.D., and Ferrell, J.E., Jr. (2003). Building a cell cycle oscillator: hysteresis and bistability in the activation of Cdc2. *Nat. Cell Biol.* 5, 346–351.
- Raj, A., van den Bogaard, P., Rifkin, S.A., van Oudenaarden, A., and Tyagi, S. (2008). Imaging individual mRNA molecules using multiple singly labeled probes. *Nat. Methods* 5, 877–879.
- Roberts, C.J., Nelson, B., Marton, M.J., Stoughton, R., Meyer, M.R., Bennett, H.A., He, Y.D., Dai, H., Walker, W.L., Hughes, T.R., et al. (2000). Signaling and circuitry of multiple MAPK pathways revealed by a matrix of global gene expression profiles. *Science* 287, 873–880.
- Rust, M.J., Markson, J.S., Lane, W.S., Fisher, D.S., and O'Shea, E.K. (2007). Ordered phosphorylation governs oscillation of a three-protein circadian clock. *Science* 318, 809–812.
- Schwob, E., and Nasmyth, K. (1993). CLB5 and CLB6, a new pair of B cyclins involved in DNA replication in *Saccharomyces cerevisiae*. *Genes Dev.* 7(7A), 1160–1175.

Sha, W., Moore, J., Chen, K., Lassaletta, A.D., Yi, C.S., Tyson, J.J., and Sible, J.C. (2003). Hysteresis drives cell-cycle transitions in *Xenopus laevis* egg extracts. *Proc. Natl. Acad. Sci. USA* **100**, 975–980.

Skotheim, J.M., Di Talia, S., Siggia, E.D., and Cross, F.R. (2008). Positive feedback of G1 cyclins ensures coherent cell cycle entry. *Nature* **454**, 291–296.

Strickfaden, S.C., Winters, M.J., Ben-Ari, G., Lamson, R.E., Tyers, M., and Pryciak, P.M. (2007). A mechanism for cell-cycle regulation of MAP kinase signaling in a yeast differentiation pathway. *Cell* **128**, 519–531.

Taberner, F.J., Quilis, I., and Igual, J.C. (2009). Spatial regulation of the start repressor *Whi5*. *Cell Cycle* **8**, 3010–3018.

Takahashi, S., and Pryciak, P.M. (2008). Membrane localization of scaffold proteins promotes graded signaling in the yeast MAP kinase cascade. *Curr. Biol.* **18**, 1184–1191.

Taylor, R.J., Falconnet, D., Niemistö, A., Ramsey, S.A., Prinz, S., Shmulevich, I., Galitski, T., and Hansen, C.L. (2009). Dynamic analysis of MAPK signaling using a high-throughput microfluidic single-cell imaging platform. *Proc. Natl. Acad. Sci. USA* **106**, 3758–3763.

Turner, J.J., Ewald, J.C., and Skotheim, J.M. (2012). Cell size control in yeast. *Curr. Biol.* **22**, R350–R359.

Tyers, M., and Futcher, B. (1993). *Far1* and *Fus3* link the mating pheromone signal transduction pathway to three G1-phase Cdc28 kinase complexes. *Mol. Cell. Biol.* **13**, 5659–5669.

Tyers, M., Tokiwa, G., Nash, R., and Futcher, B. (1992). The *Cln3-Cdc28* kinase complex of *S. cerevisiae* is regulated by proteolysis and phosphorylation. *EMBO J.* **11**, 1773–1784.

Wittenberg, C., Sugimoto, K., and Reed, S.I. (1990). G1-specific cyclins of *S. cerevisiae*: cell cycle periodicity, regulation by mating pheromone, and association with the p34CDC28 protein kinase. *Cell* **62**, 225–237.

Xiong, W., and Ferrell, J.E., Jr. (2003). A positive-feedback-based bistable ‘memory module’ that governs a cell fate decision. *Nature* **426**, 460–465.

Yeger-Lotem, E., Sattath, S., Kashtan, N., Itzkovitz, S., Milo, R., Pinter, R.Y., Alon, U., and Margalit, H. (2004). Network motifs in integrated cellular networks of transcription-regulation and protein-protein interaction. *Proc. Natl. Acad. Sci. USA* **101**, 5934–5939.

Yosef, N., and Regev, A. (2011). Impulse control: temporal dynamics in gene transcription. *Cell* **144**, 886–896.

Yu, R.C., Pesce, C.G., Colman-Lerner, A., Lok, L., Pincus, D., Serra, E., Holl, M., Benjamin, K., Gordon, A., and Brent, R. (2008). Negative feedback that improves information transmission in yeast signalling. *Nature* **456**, 755–761.